molecules

MDPI

Article

Control of the Organization of 4,4′-bis(carbazole)-1,1′-biphenyl (CBP) Molecular Materials through Siloxane Functionalization

Janah Shaya [1,2,3], Jean-Charles Ribierre [4], Gabriel Correia [1], Yannick J. Dappe [4], Fabrice Mathevet [5,6], Loïc Mager [1], Benoît Heinrich [1,*] and Stéphane Méry [1,*]

1 Institut de Physique et Chimie des Matériaux de Strasbourg (IPCMS), CNRS, Strasbourg University, UMR 7504, 23 rue du Loess, 67034 Strasbourg, France
2 Department of Chemistry, College of Arts and Sciences, Khalifa University, Abu Dhabi P.O. Box 127788, United Arab Emirates
3 College of Medicine and Health Sciences, Khalifa University, Abu Dhabi P.O. Box 127788, United Arab Emirates
4 Service de Physique de l'État Condensé, CEA CNRS UMR 3680, Université Paris Saclay, 91191 Gif-sur-Yvette, France
5 Institut Parisien de Chimie Moléculaire (IPCM), CNRS, Sorbonne University, 4 Place Jussieu, 75005 Paris, France
6 Center for Organic Photonics and Electronics Research (OPERA), Department of Applied Chemistry, Kyushu Universty, 744 Motooka, Nishi, Fukuoka 819-0395, Japan
* Correspondence: benoit.heinrich@ipcms.unistra.fr (B.H.); stephane.mery@ipcms.unistra.fr (S.M.)

Abstract: We show that through the introduction of short dimethylsiloxane chains, it was possible to suppress the crystalline state of CBP in favor of various types of organization, transitioning from a soft crystal to a fluid liquid crystal mesophase, then to a liquid state. Characterized by X-ray scattering, all organizations reveal a similar layered configuration in which layers of edge-on lying CBP cores alternate with siloxane. The difference between all CBP organizations essentially lay on the regularity of the molecular packing that modulates the interactions of neighboring conjugated cores. As a result, the materials show quite different thin film absorption and emission properties, which could be correlated to the features of the chemical architectures and the molecular organizations.

Keywords: molecular liquid; liquid crystal; siloxane side-chain; siloxane-terminated side chain; hybrid siloxane-based chain; liquid electronics; liquid emitter

Citation: Shaya, J.; Ribierre, J.-C.; Correia, G.; Dappe, Y.J.; Mathevet, F.; Mager, L.; Heinrich, B.; Méry, S. Control of the Organization of 4,4′-bis(carbazole)-1,1′-biphenyl (CBP) Molecular Materials through Siloxane Functionalization. *Molecules* **2023**, *28*, 2038. https://doi.org/10.3390/molecules28052038

Academic Editor: Borislav Angelov

Received: 23 January 2023
Revised: 10 February 2023
Accepted: 16 February 2023
Published: 21 February 2023

1. Introduction

The control of molecular organization is the object of constant and intense research activity since it determines most properties of solid-state materials. So far, a considerable amount of work has been published to describe the role of molecular parameters acting on various molecular forces and on steric effects, in particular, to try to control the solid-state molecular packing [1–4]. As an example, the substitution of organic conjugated molecules by flexible peripheral chains has become a convenient tool to control, to some extent, the molecular organization via the tuning of van der Waals interactions and steric constraints [5–7]. Until now, most of studies on side-chain functionalization have focused on alkyl chains. This is due to the wide variety of commercially available alkyl chains, including ramified ones. In comparison, very few studies have been performed with other types of chains, such as ethyleneoxide [8] or siloxane chains [9], which may induce different organization properties due to their distinctive features.

Thus, oligodimethylsiloxane (ODMS) chains -($SiMe_2$-O)$_x$- are primarily characterized by exceptional flexibility which accounts for most of their unique properties [10]. This peculiar feature arises from the nearly free torsional motion along the Si-O backbone [11]. Hence, ODMS hardly crystallizes but exhibits a strong amorphous character, as illustrated by the very low glass transition of its parent polydimethylsiloxane (PDMS) (T_g = −120 °C) [12].

Siloxane backbone also contains weak dipole moments, but the latter can easily be masked or uncovered (by an easy umbrella-type motion of the pending methyl groups), enabling ODMS to readily adapt to a polar or apolar environment [11]. Overall, ODMS possesses weak intermolecular forces entailing a very low surface tension, solubility parameter and dielectric constant, in particular [13]. In addition, ODMS is endowed with a propensity for microphase separation easily leading to the self-organization of siloxane-containing molecular systems [14–16]. Finally, with regard to geometrical parameters, siloxane chains are rather bulky, as illustrated by the larger molecular section of the linear ODMS chain (σ = 41 Å^2) as compared to the one of the linear alkyl chains (σ = 21.5 Å^2) [17].

The specific features of siloxanes have stimulated the development of many siloxane-containing organic compounds. Thus, siloxane functionalization has been applied to control the organization and tune properties of many molecular and macromolecular systems for a wide range of application domains, including optoelectronics [9,18,19]. For example, functionalization with ODMS has been used to obtain liquid crystalline organizations with favorable π-molecular interactions for charge transport properties [20]. A complex donor-acceptor (D-A) nanostructured smectic phase could even be stabilized by incorporating ODMS segments at both extremities of a D-A-D molecular triad [21,22]. A number of siloxane-hybrid side-chains conjugated polymers have also been reported to exhibit lamellar mesomorphic organization with enhanced charge transport properties (e.g., with mobilities around 1 cm^2 V^{-1} s^{-1}) [23–25]. This effect was recently attributed to the fluid and nanosegregating character of siloxane chains that impose a better facing of the polymer backbones with improved π-stacking overlap [17]. In other respects, the bulky and flexible character of ODMS has also been used to deliberately hinder π-intermolecular interactions to obtain solvent-free π-functional molecular liquids at room temperature. Thus, multiple siloxane functionalization of different arylamine and fluorene derivatives led to room-temperature liquid materials with significant charge transport and emission properties in their neat liquid phase [26,27], anticipating promising future applications of siloxane-functionalized materials in liquid (opto)electronics [28–30].

The study presented herein aims at using siloxane functionalization for tuning the molecular organization of a representative π-conjugated molecule used in optoelectronics. The objective was to scrutinize how the variation in the location and proportion of siloxane chains is able to modify and control the molecular organization from the initial system. For this study, we selected 4,4′-bis(carbazol-9-yl)biphenyl (also called CBP), a well-known carbazole-based material used as a host in organic light emitting devices [31–33]. CBP crystallizes in a herringbone-type packing and exhibits a high melting point (282 °C) [34,35]. In devices, CBP is used in its metastable glassy state obtained by chilling, but it strongly suffers from its tendency to return to its natural crystalline state [35]. Thus, rendering CBP a molecular liquid or a liquid crystal through siloxane functionalization constitutes a route toward morphologically stable guest-host devices and/or fluidic devices [29,30,36,37].

The synthetic procedure to prepare the siloxane-functionalized CBP has recently been reported elsewhere [38]. The latter focusses on the methodology we followed to introduce one or two short heptamethylsiloxane segments (via a propylene linker) at each of the carbazole end-units of CBP, to yield CBP-2Si$_3$ and CBP-4Si$_3$, respectively (Figure 1). As a preliminary result, CBP-2Si$_3$ showed a considerable drop of the melting point (T_m = 87 °C) as compared to native CBP, and CBP-4Si$_3$ exhibited a stable and fluid liquid state at room temperature, for which the only thermal event observed was a glass transition at T_g = −62 °C. These first observations already point to the considerable impact of the siloxane functionalization on the molecular organization of CBP derivatives. The aim of the present study is to undertake an extensive structural characterization by means of X-ray scattering to unravel the role of the siloxane chains on the fine molecular organization of the siloxane-functionalized CBP derivatives. In this paper, we will show in particular that the minimal insertion of siloxane in CBP-2Si$_3$ is able to stabilize a lamellar organization which can evolve up to the formation of a fluid liquid crystalline smectic phase after lengthening the siloxane chain in CBP-2Si$_n$ (with $n \approx 10$), a new compound reported herein (Figure 1).

Finally, the liquid state of CBP-4Si_3 reveals the presence of structuration at the local range that will be detailed and discussed. All these changes in molecular organization naturally impact the neat film absorption and emission properties that will also be analyzed herein, in relation to the fine molecular packing.

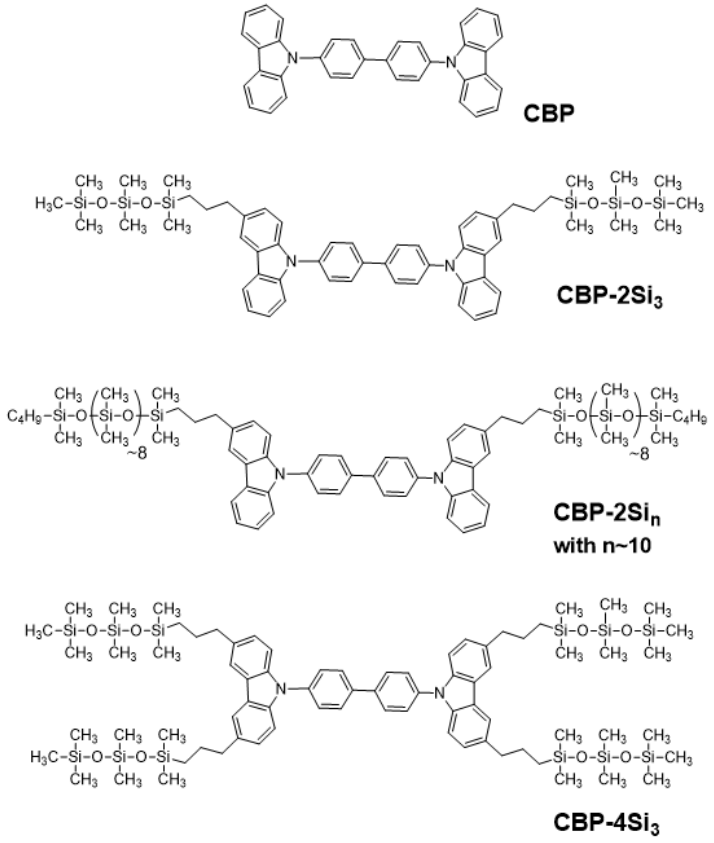

Figure 1. Structures of CBP and siloxane-functionalized CBP derivatives investigated in this study.

2. Results and Discussion

The siloxane-based CBP derivatives investigated in this study are presented in Figure 1. Molecules CBP-2Si_3 and CBP-4Si_3 are substituted by two and four short heptamethyltrisiloxane chains, respectively, while CBP-2Si_n is substituted by 2 longer oligo(dimethylsiloxane) chains (polydispersity $Đ$ = 1.2, with an average number of dimethylsiloxane units of 10, see Supplementary Materials).

2.1. Synthesis

The different siloxane-functionalized CBP derivatives investigated in this study were synthesized using optimized catalytic methodologies recently reported elsewhere (Scheme 1) [38]. Briefly, monobromocarbazole **1** was used to prepare the two CBP derivatives functionalized with two siloxane segments (short: CBP-2Si_3 and longer: CBP-2Si_n). A propylene linker was introduced to **1** via Stille cross-coupling leading to intermediate **3**. Then, **3** was reacted under Ullmann coupling conditions with dibromobiphenyl **5** to generate adduct **6**, which was further hydrosilylated with siloxane chains of different lengths to produce the final molecules CBP-2Si_3 and CBP-2Si_n. CBP-4Si_3 derivative was prepared by the same sequence of reactions using 3,6-dibromocarbazole **2** instead of monobromocarbazole. The latter synthetic route involved to double the catalytic loadings and stoichiometry of reagents in the first and third steps, leading to intermediates **4**, **7**, and the final CBP derivative (CBP-4Si_3) functionalized with 4 short siloxane segments instead of 2. The detailed synthetic protocols can be found in Ref. [38] or in the Supplementary Materials.

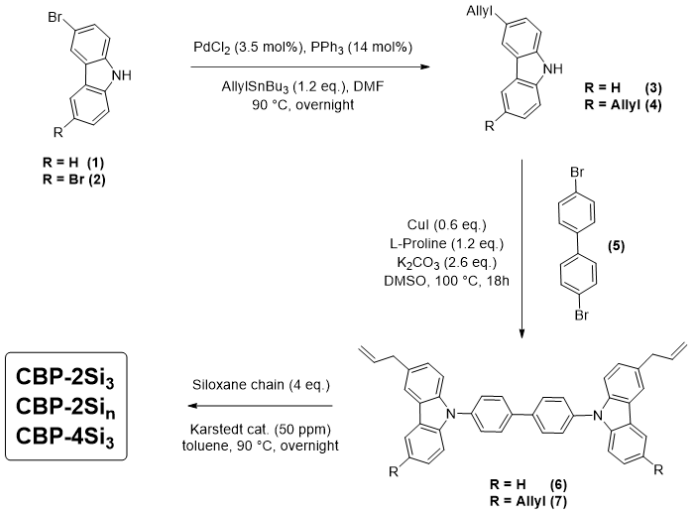

Scheme 1. Synthesis of siloxane-based CBP derivatives.

2.2. Thermal and Structural Properties

The functionalization of the CBP core by siloxane chains is found to drastically impact the organization of the materials, as CBP-2Si$_3$, CBP-2Si$_n$, and CBP-4Si$_3$ exhibit at room temperature a solid state, a liquid crystalline phase, and a liquid state, respectively. Table 1 summarizes the transition temperatures and the enthalpy changes, issued from differential calorimetry (DSC) and thermogravimetry (TGA) analyses, shown in Figures 2 and S5 (Supplementary Materials), respectively.

Table 1. Phase behavior with transition temperatures and enthalpies associated in the CBP materials series.

Compound	T_g (°C)	T_m (°C)	$T_{LC\rightarrow Iso}$ (°C)	$\Delta H_{\rightarrow Iso}$ (kJ/mol)	T_{deg} (°C)
CBP [35]	(62)	282	-	40	365
CBP-2Si$_3$	-	87	-	16	250
CBP-2Si$_n$	-	-	27	11	270
CBP-4Si$_3$	−60	-	-	0	250

T_g, glass transition temperature; $T_{LC\rightarrow Iso}$, transition temperature from the liquid crystal phase to the isotropic liquid; T_m, melting point; $\Delta H_{\rightarrow Iso}$, enthalpy change associated with the transition toward the isotropic liquid phase; T_{deg}, degradation temperature corresponding to a 5% weight loss temperature, under air.

To start with thermal stability, the siloxane chain functionalization lowers the materials stability as T_{deg} is decreased by about 100 °C for all siloxane-based CBP derivatives as regards to reference CBP. Next, we examine the effect of siloxane chain substitution on the organization of the CBP materials (See Table 1). The introduction of two short siloxane chains is sufficient to strongly destabilize the crystal state, as T_m is decreased from 282 to 87 °C when transitioning from CBP to CBP-2Si$_3$. The destabilization is further aggravated by lengthening the siloxane chain, the crystalline state being replaced by a room-temperature liquid crystalline phase (clearing temperature: $T_{LC\rightarrow Iso}$ = 27 °C) in CBP-2Si$_n$. Finally, the substitution of four short siloxane chains totally suppresses any long-range order in the packing of the CBP core, leading to a room-temperature liquid state with a sub-ambient glass transition temperature ($T_g \approx -60$ °C) in CBP-4Si$_3$. The destabilizing effect of the siloxane functionalization is well illustrated by the strong decrease of the enthalpy change, $\Delta H_{\rightarrow Iso}$ (associated with the transition toward this isotropic liquid phase), observed in the CBP materials series. This value is found to drop stepwise when transitioning from the crystal CBP (40 kJ mol^{-1}), the solid state CBP-2Si$_3$ (16 kJ mol^{-1}), the liquid crystalline CBP-2Si$_n$ (11 kJ mol^{-1}), down to the glassy CBP-4Si$_3$ (0 kJ mol^{-1}). The states of the CBP derivatives have been primarily assigned after polarized microscopic observation (POM). For CBP-2Si$_n$, the liquid crystal phase is clearly evidenced by the POM

texture obtained under crossed polarizers shown in Figure 3. The fluid focal-conic domain texture observed gives indication of the presence of a uniaxial lamellar mesophase.

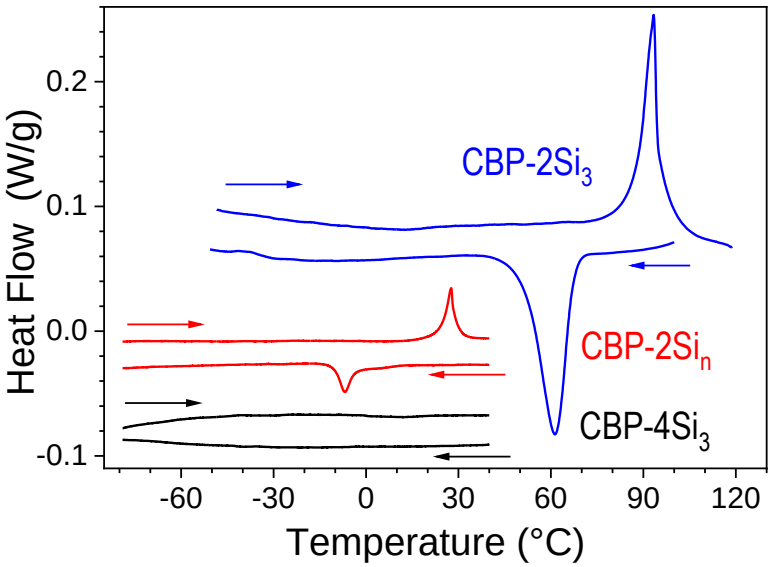

Figure 2. DSC traces of the siloxane-functionalized CBP derivatives, recorded at 5 °C min^{-1}, on first cooling and second heating (endotherm up). The DSC data of CBP-$2Si_3$ and CBP-$4Si_3$ were already shown in the precedent article [38].

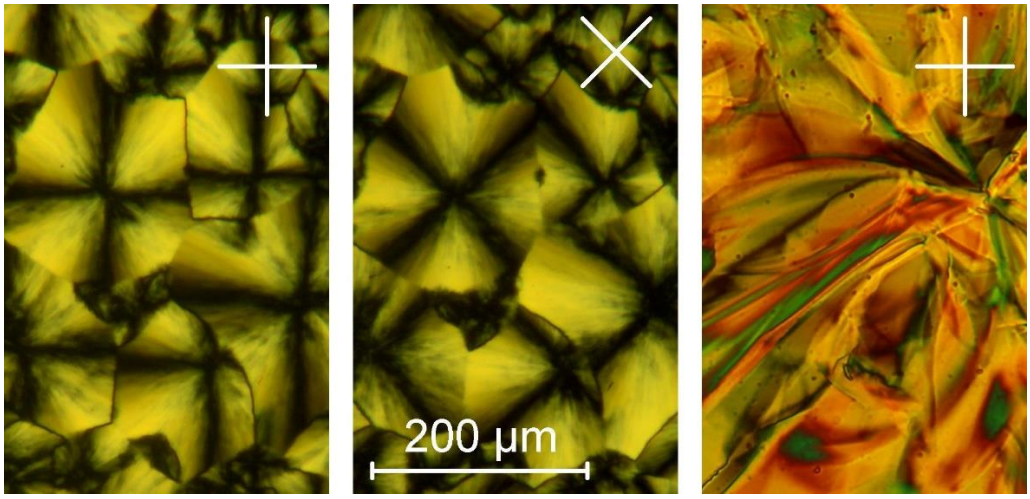

Figure 3. Polarizing optical microscopy observation of the room-temperature mesophase of CBP-$2Si_n$ (**left**,**middle**) and of the soft crystalline phase of CBP-$2Si_3$ (**right**); the white crosses give the directions of the crossed polarizers. The fluid focal-conic domain texture observed of CBP-$2Si_n$ indicates the presence of a uniaxial lamellar mesophase. The highly viscous mosaic texture of CBP-$2Si_3$ is indicative of a phase with high degree of long-range positional ordering.

The fine structural organization of the siloxane-functionalized CBP derivatives has been extensively investigated by small- and wide-angle X-ray scattering (SWAXS) and grazing incidence wide-angle X-ray scattering (GIWAXS). Representative SWAXS patterns recorded for all materials at room temperature are presented in Figure 4a–d. The GIWAXS patterns specifically recorded for CBP-$2Si_3$ are shown in Figure 5 (room-temperature) and Figure S6 (100 °C), respectively. A compilation of the structural parameter data can be found in Supplementary Materials.

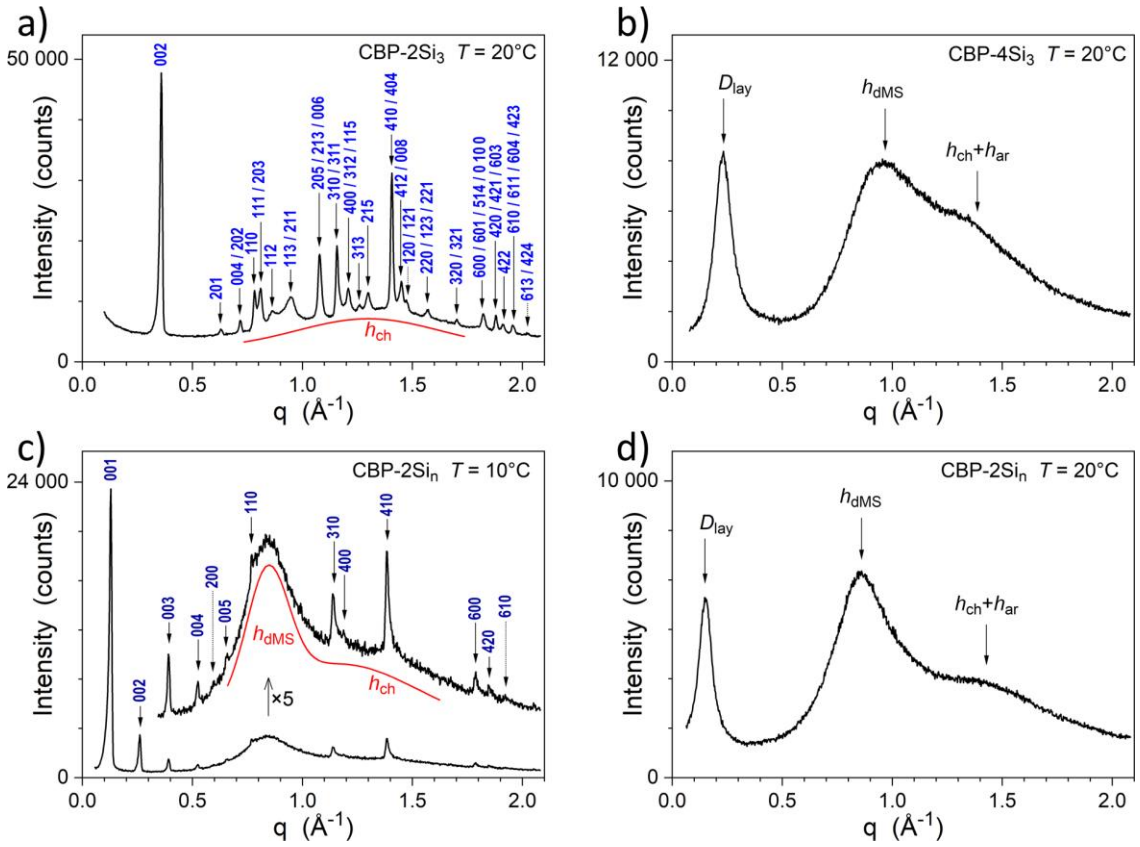

Figure 4. SWAXS patterns of the CBP materials recorded at room temperature: (**a**) CBP-2Si$_3$ (solid state at 20 °C), (**b**) CBP-4Si$_3$ (liquid phase at 20 °C), (**c**) CBP-2Si$_n$ (mesophase at 10 °C) and (**d**) CBP-2Si$_n$ (supercooled liquid phase at 20 °C).

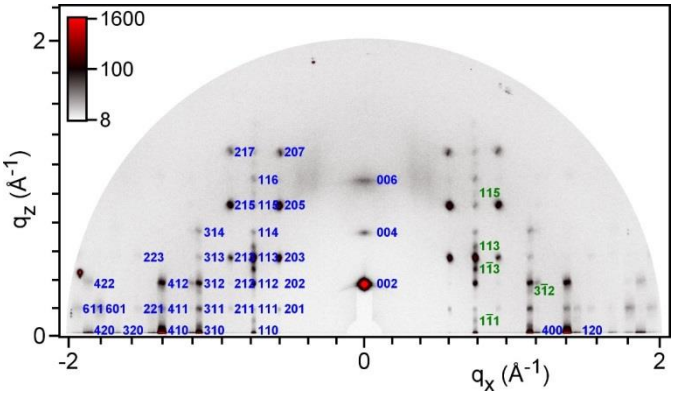

Figure 5. GIWAXS pattern of a CBP-2Si$_3$ layer spin-coated onto Si wafer recorded at room temperature. This pattern displays an orthorhombic structure equivalent to the one recorded by SWAXS for the bulk material (blue labels). Here, some weak satellite spots become visible (green labels) and reveal the coexistence with a monoclinic modification, in an amount of approximately 20% (as deduced from spot integration). Except for the non-orthogonal angle, the lattice parameters are nearly unchanged with respect to the orthorhombic cell (a = 20.8(3) Å, b = 8.79 Å, c = 34.2(74) Å, α = 96.1°, V = 6240 Å^3 (Z = 4)) and the structure just differs by a regular 1.8 Å shift along b-axis of the successive lamellae.

Examining the SWAXS pattern of CBP-2Si$_3$ (at 20 °C), shown in Figure 4a, this pattern displays many sharp reflections in the whole angular range together with a broad scattering signal from lateral interactions of molten alkyl chains (h_{ch}). This information indicates a soft-crystalline organization, in which crystal-like, three-dimensional long-range ordering

of conjugated segments coexists with molten chain zones [39–41]. Structural features could be specified through the combination with an oriented GIWAXS pattern obtained for a spin-coated thin film of CBP-2Si$_3$ (see Figure 5). Thereby, the structure and morphology of the film was lamellar with the layers oriented parallel to the substrate. The direction of the normal layer was identified to the *c*-axis of an orthorhombic structure, designed by the in-plane arrangement and the superposition of layers. The lattice parameters are reported in Table S1. The cell periodicity involves two lamellae with a staggered superposition causing the extinction of (00*l*) reflections with odd *l* value; the lamellar periodicity is hence: $d_{lam} = d_{002} = 17.25$ Å. The in-plane arrangement follows an **a** × **b** sublattice of *p*2*mg* or *p*2*gg* symmetry that involves $Z_{2D} = Z/2 = 2$ molecular stacks covering an area $A/Z_{2D} = ab/2 = 91.0$ Å^2 (cf. Table S1). In addition to that of odd (00*l*), one notices the extinction of reflections (*h*00) and (*h*0*l*) with odd *h* value. Three space groups are then compatible with this composition of patterns: *Pca*2$_1$, *Pna*2$_1$, and *Pbcm*.

Figure 4b presents the SWAXS pattern of the liquid CBP-4Si$_3$ recorded at 20 °C. A similar pattern was obtained for CBP-2Si$_3$ in its high temperature (100 °C) liquid state (see Figure S6). Both patterns show the same distinct scattering signals for siloxane segments (h_{dMS} = 6.5–7 Å), and aliphatic or CBP segments (h_{ch} + h_{ar} = 4.5–5 Å), demonstrating the persistence of nanosegregated strata in the liquid state. The periodicity of the strata alternation leads to a further scattering signal in the low-angle region (D_{lay} = 29 and 27 Å, for CBP-2Si$_3$ and CBP-4Si$_3$, respectively, with similar correlation length $\xi \approx 60$ Å obtained from full width half-maximum *FWHM* and Scherrer formula $\xi = K\,2\pi/\Delta q$ with $\Delta q = (FWHM^2 — FWHM_0{}^2)^{0.5}$, beam width $FWHM_0 = 0.006$ Å^{-1} and shape factor $K = 0.9$).

Figure 4c,d show the SWAXS patterns of CBP-2Si$_n$ after different thermal treatments. They correspond to a record of the material at 10 °C in the mesophase (Figure 4c), and after heating to isotropic liquid down to the supercooled isotropic liquid at 20 °C (Figure 4d). First, the mesophase pattern (Figure 4c) indicates a mesophase with a smectic E-analogue structure, with lamellae constituted by the alternation of molten chain layers and layers of mesogens arranged in a long-range correlated two-dimensional rectangular lattice (lamellar periodicity: $d_{lam} = d_{001} = 48.1$ Å). The presence of the molten chain sublayers is indeed demonstrated by their characteristic signatures h_{dMS} and h_{ch}. The lattice geometry and reflection intensity ratios of CBP-2Si$_n$ are comparable to the *p*2*mg* **a** × **b** sub-lattice of the soft crystal phase of CBP-2Si$_3$, indicating the similarity of the molecular organizations, notwithstanding the loss of the three-dimensional superstructure as a result of the thick siloxane layer intercalation. Due to its low clearing temperature (24 °C), CBP-2Si$_n$ stays for days in the isotropic liquid phase at room-temperature once melted. Then, the SWAXS pattern recorded in its supercooled liquid state at 20 °C (see Figure 4d) is very similar to the one of CBP-2Si$_3$ and CBP-4Si$_3$ in their isotropic liquid phase, as shown in Figures S6 and 4b, respectively. Because of the high proportion of siloxane chains in CBP-2Si$_n$, its liquid state gives higher layer periodicity (D_{lay} = 42 Å) and correlation length ($\xi \approx 100$ Å), as CBP-2Si$_3$ and CBP-4Si$_3$ in their liquid phase (compare with D_{lay} = 27–29 Å, and $\xi \approx 60$ Å).

The combination of the results obtained by SWAXS measurements and by geometrical calculations gave access to a number of structural parameters (see Tables S1 and S2 in Supplementary Materials) allowing us to fully describe the molecular organization of the CBP derivatives in the different phases. First, let us consider the molecular organization of CBP-2Si$_3$ in its soft crystal phase. Actually, the CBP core has a shape of a dumbbell of approximately 19 Å length and 9 Å width (both including the van der Waals radii), with lateral close-packing distances in the order of 4 Å, while siloxane units can be approximated by cylinders of 7–7.5 Å diameter. The nanosegregation of both moieties (i.e., aromatic core and siloxane chains) into lamellae implies that the molecular area of the sequence of layers fits the individual space requirements, which is realized by the interdigitation of the siloxane end-segments. The different types of self-arrangements (namely, rows aligned on the *a*-axis and spaced by $b/2 = 4.3$ Å for CBP, and close-packed cylinders for siloxane chains), are however mutually constrained by the interconnecting propylene spacer. Therefore, the successive rows constituting the CBP layers are longitudinally shifted along the *a*-axis to

allow the close-packing of siloxane chains, which determines the in-plane periodicity of two rows along the *b*-axis. Additionally, the interdigitation of the side-chains imposes a staggered superposition of successive CBP layers and thus the periodicity of two molecular layers along the *c*-axis. These constraints result in an original *p2mg* arrangement of CBP cores and a cohesive three-dimensional structure of $Pca2_1$ symmetry (Figure 6), which is consistent with the selected space groups.

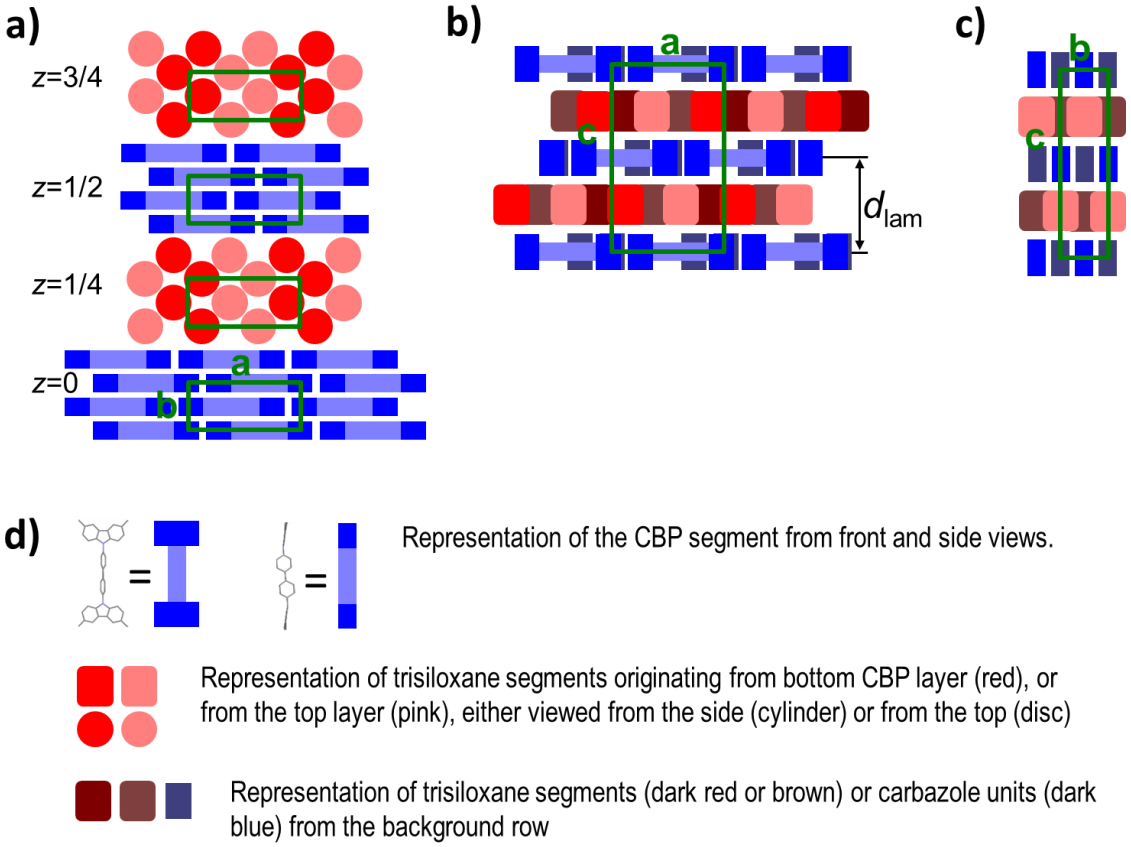

Figure 6. Structural model of the molecular organization of CBP-2Si_3 in the soft-crystal phase (**a**–**c**) and definition of the different molecular subunits (**d**). The molecular geometry of the CBP segment was extracted from the single-crystal structure CSD-WETFOS [42].

The organization of CBP derivatives evolves significantly with siloxane chain content. The molecular self-organization can thus be controlled through the siloxane chain functionalization, as illustrated in Figure 7. Due to the lower cross-sectional area of the siloxane chain (about two-fold smaller) as compared to the CBP core, the two trisiloxane chains in CBP-2Si_3 form intercalated monolayers that alternate with CBP monolayers. This intercalation strongly constrains the respective positions of segments from different layers, which explains the evolution of the lamellar structure into a cohesive three-dimensional soft-crystal. Conversely, these constraints are removed with the four chains of CBP-4Si_3 and the disentanglement of the siloxane segments, resulting in a single liquid phase. On the other hand, the use of longer siloxane chains for CBP-2Si_n blurs the three-dimensional structure interconnecting CBP segments, while reinforcing the nanosegregation into layers. This results in the substitution of the lamellar soft-crystal by a smectic-like mesophase. As a side-effect, however, a lateral shrinking of the siloxane layers (and thus of the entire lamellae) is observed, in relation to the polydispersity of the long siloxane chains, that mimic a partial bilayer configuration. More detailed structural information can be found in the Supplementary Materials (Tables S1 and S2 and Figure S7).

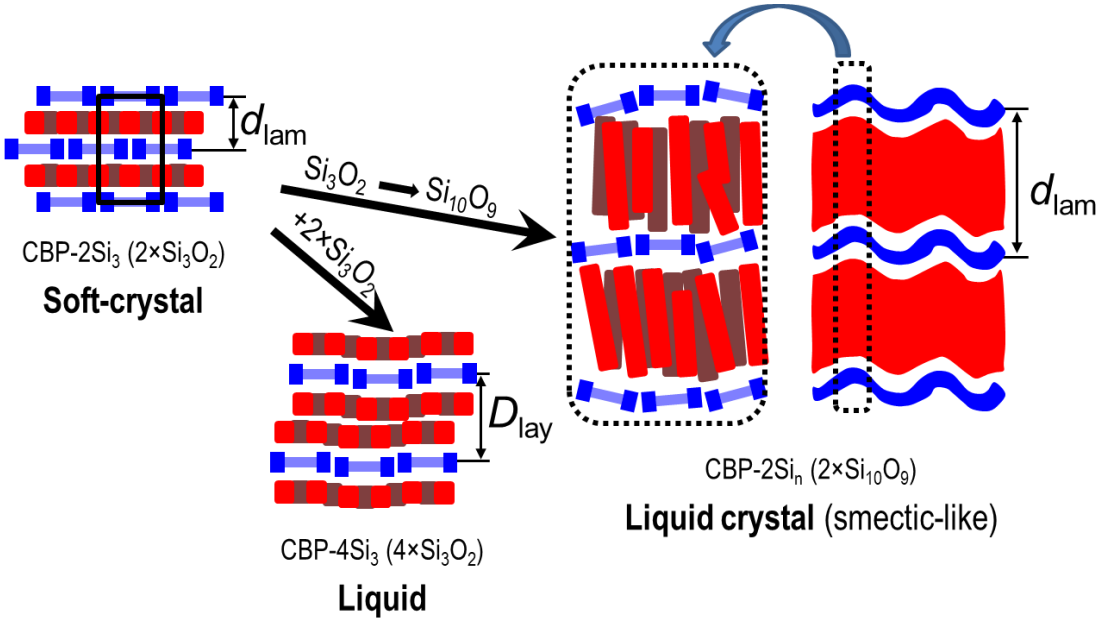

Figure 7. Evolution of the self-organized structures of the CBP derivatives, as a function of the siloxane chains content, as obtained from structural modeling based on pattern information and molecular segment geometry [43–46].

It is worth noting that the lamellar structure observed for all siloxane-functionalized CBP molecules differs quite significantly from the unsubstituted CBP crystal structure. Actually, neat CBP molecules self-assemble into herringbone rows along which the carbazole rings stack into columns [47]. Successive herringbone rows then fit one into the other with close-packing of the carbazole and biphenyl units, as illustrated in Figure 8. The whole results clearly demonstrate the strong microsegregation ability of siloxane chains which is able to impose, not only the lamellar organization of the molecules but also the lateral packing of the CBP cores, by forcing molecular interactions through carbazole units. Siloxane chain functionalization then constitutes a powerful tool to control molecular arrangement and molecular packing. Depending on the location, number, and length of the siloxane chain, it is possible to tune the organization of the molecules and their molecular interactions.

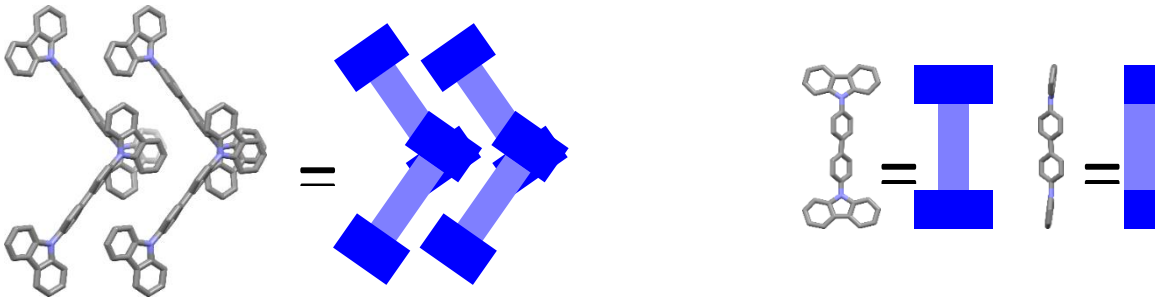

Figure 8. Molecular geometry of neat (unsubstituted) CBP molecules in the single-crystal structure CSD-KANYUU [47] and schematic representation of CBP from front and side views.

Lastly, the spontaneous alignment observed for the siloxane-functionalized solid-state CBP derivatives should be addressed. Actually, when CBP-2Si_3 was deposited as a thin film by spin coating, the siloxane layer planes were found to spontaneously align parallel to the substrate. This effect is most likely driven by the very low surface energy of ODMS (around 20–22 mN m^{-1}) [13]. Siloxane-containing molecular systems should minimize their energy by preferably orienting the siloxane chains at the interface with air (and probably with the glass substrate also), thereby imposing the orientation of the lamellar organization parallel

to the substrate on the whole film thickness [48,49]. Siloxane-functionalization then turns out to be a valuable tool for controlling the morphology of functional organic materials.

2.3. Photophysical Properties in Solution

The photophysical properties of the dyes were inspected in a dichloromethane solution (Figure S9). The absorption peaks observed in CBP at 340 and 293 nm are associated with transitions localized on the carbazole units while the additional absorption band at 317 nm is attributed to transitions involving the central benzidine group [35]. As stated in another study [50], the presence of both carbazole and benzidine characteristics in the absorption spectrum of CBP indicates that the electron density in the ground state is delocalized over the whole chromophore. As can be seen in Figure S9, the UV-visible absorption spectra of the different CBP functionalized with the siloxane chains are rather similar to that of CBP. This implies that the functionalization of the siloxane side chains on the carbazole units does not significantly affect the delocalization of the electron density in the ground state. The only differences appear on the redshift of the lowest absorption bands in energy when transitioning from CBP to CBP-2Si_3 (or CBP-2Si_n) to CBP-4Si_3. As shown in Figure S9, a gradual red-shift of the emission spectra is also observed when transitioning from CBP to CBP-2Si_3, CBP-2Si_n, and CBP-4Si_3. The fluorescence properties of CBP involve predominantly the central benzidine part of the molecule and exhibit some charge transfer character that can make it sensitive to the polarity of the environment [50]. However, previous studies have shown that the siloxane chains present a low polarity, similar to that of alkane chains [51], and we thus exclude changes in the polarity of the local environment as a reason for the different photophysical properties of the siloxane-based compounds. To gain further insights, quantum chemistry calculations were carried out to estimate the highest occupied molecular orbital (HOMO) and lowest unoccupied molecular orbital (LUMO) distributions, oscillator strengths and the first excited-state singlet energies in CBP and CBP functionalized with 2 and 4 propyl side chains (CBP-2prop and CBP-4prop, respectively) in the gas phase using time-dependent density functional theory (TD-DFT) with the B3LYP functional in the 6–31 G basis. Siloxane chains were removed for these calculations to reduce their computing time. In good consistency with a previous study devoted to CBP derivatives [52], it can be seen in Figure 9 that the HOMOs of CBP, CBP-2prop, and CBP-4prop are delocalized over the whole molecules while their LUMOs are localized mainly onto the central biphenyl. Substituting propyl side chains to the carbazole units of the CBP core is also found to hardly affect the dihedral angle at the ground state between the phenyl rings (36.4° for CBP, 36.3° for CBP-2prop and 36.2° for CBP-4prop). More noticeably, this substitution leads to some changes in HOMO/LUMO energy levels and to a gradual decrease in the singlet energy together with a slight increase in the oscillator strength (see Table 2). Overall, these calculations suggest that the small redshift of both absorption and steady-state emission spectra in Figure S9 should not be attributed to a change of planarization of the molecules, but rather to the variation in their electronic properties induced by the electro-donating character of the grafted chains.

Table 2. Calculated energy levels of CBP, CBP-2prop and CBP-4prop using a TD-DFT method (B3LYP, 6–31 G) in the gas phase.

	CBP	**CBP-2prop**	**CBP-4prop**
LUMO (eV)	1.23	1.20	1.16
HOMO (eV)	5.32	5.22	5.13
S_1 (eV)	3.56 *	3.50 *	3.46 *
$\lambda_{S0\text{-}S1}$ (nm)	348	354	359
Oscillator strength	0.6417	0.6918	0.7463

* These values are in good agreement with the experimental optical bandgaps determined from the solution UV-Vis spectra of CBP (3.52 eV), CBP-2Si_3 (3.45 eV) and CBP-4SI_3 (3.41 eV) (see Figure S9).

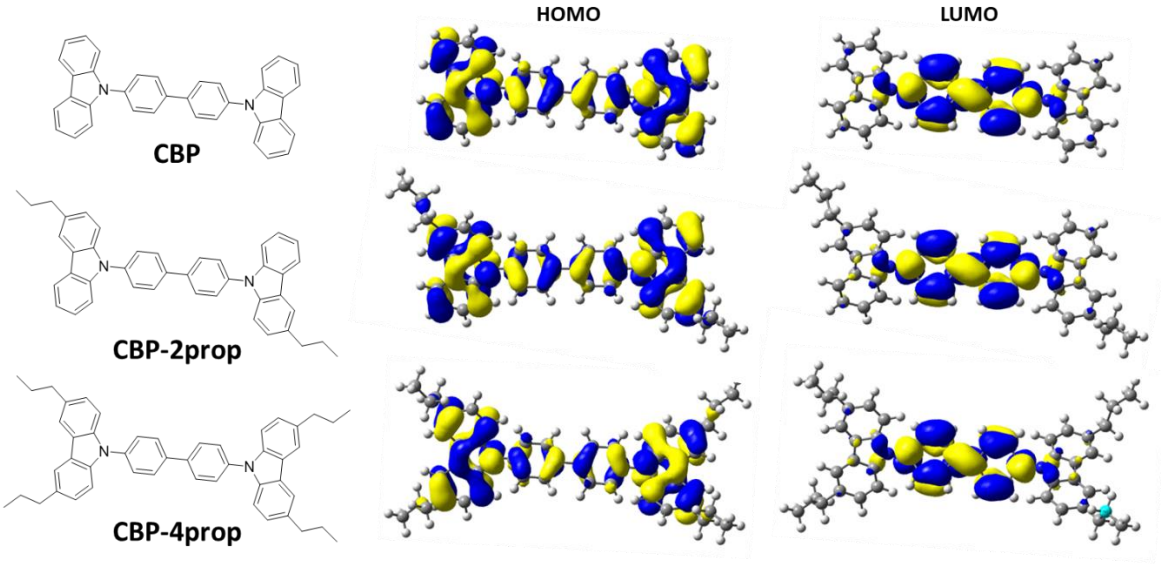

Figure 9. Molecular structures and HOMO/LUMO distributions of CBP, CBP-2prop and CBP-4prop.

2.4. Photophysical and Charge Transport Properties in Thin Films

The functionalization of the CBP molecule by the siloxane hybrid side-chains has been found to strongly modify the structural properties in thin films, which, in turn, should have a significant impact on their photophysical and charge transport properties. Figure 10 displays the thin film UV/visible absorption spectra of the siloxane-functionalized CBP derivatives with their different phases, as well as of the neat CBP in its glassy amorphous and crystal states. The glassy amorphous CBP film was obtained immediately after spin-coating deposition of the CBP solution in 1 wt.% chloroform, while the crystalline state was formed after allowing the same film to stand for more than one day at room temperature. All data in solution and solid state are summarized in Table 3.

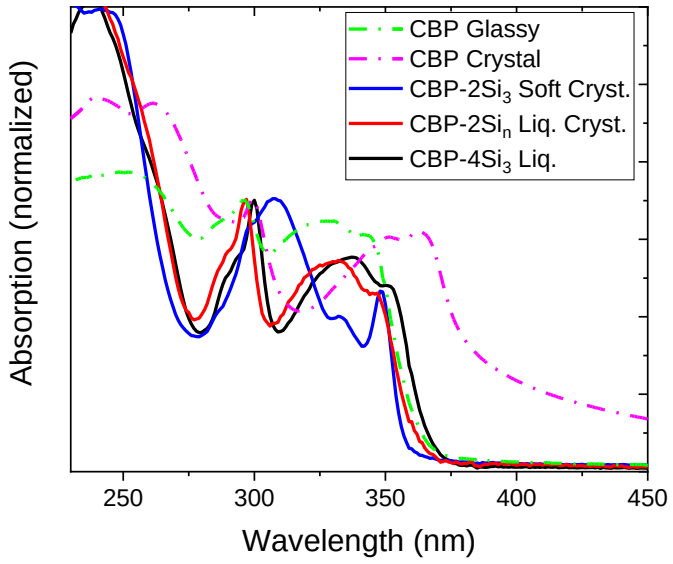

Figure 10. Absorption spectra of the CBP derivatives in thin films.

Table 3. Absorption and emission data of the CBP derivatives, recorded in solution and in thin film.

Compound		Absorption		Emission		
Name	**State**	λ_{max} **(sol.)** [a] **(nm)**	λ_{max} **(film) (nm)**	λ_{max} **(sol.)** [a,b] **(nm)**	λ_{max} **(film)** [b] **(nm)**	*PLQY* [c] **(%)**
CBP	**Glassy**	293, 317, *340* *	299, 351, 363	372	362, *384* *	0.51
	Crystal		299, 351, 363		372, 388, *409* *	0.36
CBP-4Si$_3$	**Liquid (smectic-like) liquid crystal**	300, 333, *351* *	308, 333, *348* *	395	*377*, *392* *	0.58
CBP-2Si$_{10}$		296, 326, *346* *	297, 332, *347* *	385	374, *389* *	0.35
CBP-2Si$_3$	**Soft crystal**	296, 325, *347* *	300, 338, 352	376	354, 366	0.16

[a] in dichloromethane at 10^{-5} M; [b] after excitation at 310 nm; [c] averaged value after excitations at 290, 310 and 330 nm. * shoulder.

Unlike the results obtained in solution (Figure S9), the absorption and photoluminescence spectra in thin films that are displayed in Figures 10 and 11 show significant differences depending on the nature of their condensed phase. The absorption spectrum of the crystalline CBP thin film exhibits a substantial redshift compared to its glassy film with a tail at longer wavelengths, which can be explained by the particular CBP molecular packing and the possible contribution of scattering by small crystallites [53]. Noticeably, the absorption spectrum of the soft crystal CBP-2Si$_3$ film shows different features compared to that of crystalline CBP. In contrast to what is observed in dichloromethane solution, the relative intensity of the absorption bands in CBP-2Si$_3$ film is modified with, in particular, a decrease in the absorption of the peak associated with the benzidine unit together with a hypsochromic shift. When compared to the spectra of the two other siloxane-containing CBPs, soft-crystal CBP-2Si$_3$ also shows a different absorption spectrum with more intense bands at 300 and 347 nm, which are characteristics of the carbazole unit. By contrast, CBP-4Si$_3$ and CBP-2Si$_n$ spectra are very similar indeed and strongly resemble all CBP derivatives spectra measured in solution (Figure S9). This is presumably due to the rather weak intermolecular interactions between aromatics cores taking place in the liquid state and the fluid mesophase (Figure 7). Finally, the absorption spectrum of the non-functionalized CBP in its glassy amorphous state strongly resembles the ones of the "fluid" siloxane-functionalized CBP derivatives CBP-4Si$_3$ and CBP-2Si$_n$.

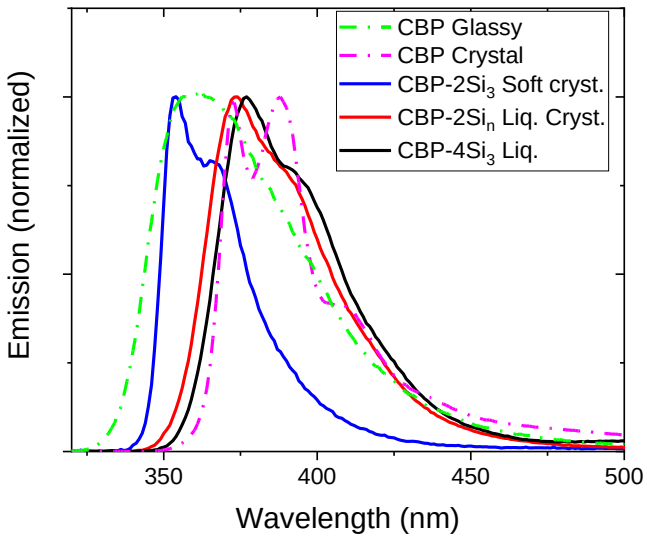

Figure 11. Normalized steady-state emission spectra of CBP derivatives in thin films measured using an excitation wavelength of 310 nm.

Figure 11 displays the steady-state photoluminescence spectra of the CBP derivatives in thin films. Compared to the CBP glassy film, the emission spectrum of the CBP crystal exhibits a substantial redshift together with a well-resolved vibronic structure exhibiting two vibronic peaks and one shoulder in the range between 370 and 410 nm. Noticeably, the fluorescence spectra of both CBP-2Si$_n$ and CBP-4Si$_3$ show similar features (see Table 3) and the slight red-shift of the emission of CBP-4Si$_3$ is presumably due to the effects of the two additional electron-donating side chains in CBP-4Si$_3$ as compared to CBP-2Si$_n$ on the electronic properties, similarly to what is observed in solution. The most intriguing result in Figure 11 comes from the emission spectrum of CBP-2Si$_3$. While its emission spectrum shows the same vibronic structure as the other siloxane-containing CBP derivatives, the emission of CBP-2Si$_3$ is blue-shifted by more than 20 nm. Carbazole derivatives are known for their tendency to form excimers in which interacting carbazole units are stacked in an overlapping sandwich-like configuration [54]. However, the fluorescence of CBP is dominated by the properties of the central biphenyl part of the molecule and it has been shown that this compound does not exhibit excimer emission in thin films [52]. In addition, the fluorescence of highly twisted CBP derivatives was found to be dominated by the individual properties of the *N*-phenylcarbazole units and to show a significantly blue-shifted emission as compared with the spectrum of CBP films [52]. In this context, the most plausible explanation for the blue-shift of the emission is that CBP-2Si$_3$ molecules adopt in the condensed phase a more twisted geometry with a larger torsion angle between the two phenyl rings of the benzidine core. This would also be consistent with the observed decrease in the absorption band of the benzidine moiety in the absorption spectrum of CBP-2Si$_3$ film and with the fact that the thin film shows a blue shifted emission as compared to the solution [55]. It should also be emphasized that the X-ray scattering results indicated that the structure and morphology of the CBP-2Si$_3$ film is lamellar with layers oriented in the direction parallel to the substrate. The interactions within the layers of aggregated CBP rings affect the emission with respect to isolated molecules in solution [56]. Additionally, there might also be an impact of molecular architecture and packing on the dihedral angle between the two *N*-phenylcarbazole units. To gain further insights, we looked at the molecular geometry at the DFT level in order to examine the potential energy landscape of the CBP-2Si$_3$ molecule (Figure S10). The most stable molecular geometry is obtained for an angle around 30°, which is in good consistency with a previous report devoted to CBP [52]. However, the calculations show that there is another energetically favorable minimum for an angle around 50° and it is, therefore, possible that the average dihedral angle in CBP-2Si$_3$ films deviates from the average value in solution, which could explain a part of the frequency shift.

The photoluminescence quantum yield (*PLQY*) of the CBP derivatives was then measured in thin films. As displayed in Table 3, the siloxane-functionalized CBP series show a substantial decrease in PLQY as the degree of order increases, from 0.58 (Liquid), 0.35 (Liquid crystal) to 0.16 (Soft crystal). However, soft crystal CBP-2Si$_3$ gives a lower *PLQY* than classical crystal CBP (0.36), which means that molecular organizations and conformations in both systems have different efficiencies upon luminescence quenching. If we compare the molecular organization in CBP and CBP-2Si$_3$, which are schematically represented in Figures 7 and 8, the herringbone organization in the CBP crystal might involve a lower aromatic core overlap and thus a weaker quenching of the emission due to intermolecular interactions. In addition, the twisting of the benzidine core suggested by the absorption and steady-state fluorescence spectra of CBP-2Si$_3$ would presumably lead to a reduction in the oscillator strength and a substantially lower *PLQY* value. Regarding the liquid crystalline CBP-2Si$_n$, the CBP cores in this system self-arrange in a similar way as CBP-2Si$_3$ but the efficiency of the benzidine core interactions and ultimately the quenching is altered by the less regular smectic in-plane order. Finally, these interactions are further reduced in the liquid phase, leading to the highest *PLQY* for CBP-4Si$_3$. The luminescence of this liquid material even overcomes that of glassy amorphous CBP, for which *PLQY* is also enhanced by structural disorder, relative to crystalline CBP.

The CBP molecule has been intensively used as a host material in organic light-emitting diodes [57] and its neat film shows hole and electron mobilities on the order of 10^{-3}–10^{-4} cm^2 V^{-1} s^{-1} [58,59]. A previous work has characterized the charge carrier mobilities of siloxane-containing oligofluorene derivatives using the time-of-flight technique (ToF). The electron and hole mobilities in liquid oligofluorene were found to be on the order of 10^{-4} cm^2 V^{-1} s^{-1} and comparable with the values measured in solid thin films of other fluorene derivatives [27]. In this context, it was relevant to characterize the charge transport properties of the siloxane containing CBPs but, in contrast with what was observed in liquid fluorene derivatives, their investigation by ToF turned out to be unsuccessful (see Supplementary Materials). The measurements carried out on commercial ITO-covered liquid crystal cells filled by capillarity with materials in their liquid state only led to a poor response indicating a low charge carrier mobility with estimated values well below 10^{-6} cm^2 V^{-1} s^{-1} for all materials. Regarding the soft crystalline CBP-2Si_3, the film shows no domain orientation when implemented as the semiconducting layer of the measuring device. Charge transport of CBP-2Si_3 was therefore jeopardized by the insulating siloxane layers interrupting the conduction pathways towards electrodes. In the case of CBP-4Si_3, it can be assumed that the significantly reduced intermolecular interactions between CBP units, as confirmed by its high *PLQY* value, lead to poor conductive pathways. The same effect presumably occurs for CBP-2Si_n in conjugation with the dilution of the low-efficient conduction pathways in the high-volume fraction of insulating siloxane.

The results obtained in this study indicate that these CBP derivatives exhibit promising photophysical properties for organic optoelectronics, but their potential use is still strongly limited by their charge transport properties. One aspect potentially detrimental to charge transport in the liquid and liquid crystal states of these systems is the location of the siloxane chains onto the carbazole end units. By considering the molecular organization as depicted in Figure 7, it is possible that the insertion of voluminous side chains directly to the carbazole end units alter the efficiency of conduction pathways by reducing the π-orbital overlap between carbazole units. Consequently, there is still a possibility to improve the molecular design and get liquid or liquid crystalline CBPs with enhanced charge transport performances.

3. Conclusions

Siloxane substituents can be seen as an alternative to alkyl chains for the control of the molecular organization in organic thin films. Thus, by functionalizing π-conjugated molecules with siloxane chains, mesomorphic organizations are readily obtained by innate segregation between the siloxane chains and the conjugated units. At the same time, crystallization is drastically hindered, usually in favor of a glass transition at a very low temperature, leading to the formation of soft and fluid material in an ambient environment. In a previous work, we demonstrated that CBP, a conjugated molecule of interest for organic optoelectronics and well-known in the area of OLEDs, could become liquid at room temperature through the introduction of siloxane-terminated side-chains, whereas the unsubstituted material is crystalline and melts at 270 °C. In the present study, the design of the siloxane side-chains allowed to vary the self-organization of the materials between a three-dimensional lamellar soft-crystal with two short siloxane chains, a nanosegregated liquid freezing only at −62 °C with four chains, and a room-temperature smectic liquid-crystal with two longer chains. The photophysical properties of the films were then investigated in the different materials and could be correlated to their molecular organizations. In particular, the liquid CBP functionalized with four siloxane chains was found to exhibit a *PLQY* of 58%, higher than that of glassy CBP, due to a reduction in the intermolecular interactions between neighboring conjugated cores. However, the results also indicate that those siloxane-containing CBP derivatives exhibit poor charge transport properties, which seriously limit for now their potential use in organic optoelectronics. While the outcome of this work is highly relevant for rationalizing the role of siloxane chain functionalization in the control of the molecular organization, further efforts are still required in terms of

molecular design to obtain high-performance functional siloxane containing optoelectronic materials based on a CBP core.

Supplementary Materials: The following supporting information can be downloaded at: https://www.mdpi.com/article/10.3390/molecules28052038/s1, Figure S1: Size exclusion chromatography (SEC) of the starting oligo(dimethylsiloxane) chains (MCRH11 from Gelest) used in the synthesis of CBP-2Si$_n$. Elution in toluene with PDMS standards; the peak indicated at 35 mL indicates the octamethylcyclotetrasiloxane reference (D4); Figure S2: ^{1}H NMR spectrum of CBP-2Si^n recorded in $CDCl_3$; Figure S3: ^{13}C NMR spectrum of CBP-2Si$_n$ recorded in $CDCl_3$; Figure S4: Maldi-ToF MS spectrum of CBP-2Si$_n$; Figure S5: TGA thermograms of CBP and CBP derivatives recorded at 5 °C min^{-1}; Figure S6: SWAXS patterns recorded in the liquid phase of CBP-2Si$_3$ (at 100 °C). This pattern is similar than the one of CBP-4Si$_3$ recorded in its liquid state at 20 °C. Both patterns show distinct scattering signals for siloxane segments (h_{dMS} = 6.5–7 Å), and aliphatic or CBP segments (h_{ch} + h_{ar} = 4.5–5 Å), demonstrating the persistence of nanosegregated strata in the liquid state. The periodicity of the strata alternation leads to a further scattering signal in the low-angle region (D_{lay} = 29 and 27 Å, for CBP-2Si$_3$ and CBP-4Si$_3$, respectively, with similar correlation length $\xi \approx 60$ Å, determined from Scherrer formula with shape factor K = 0.9; Figure S7: Illustration of the evolution of the self-organized structures of the CBP derivatives as a function of the siloxane chains content, including molecular parameters issued from Table S5; Figure S8: Left: SWAXS patterns of the CBP-2Si$_3$ in the pristine state at 20 °C (black curve) and in the supercooled liquid phase at 20 °C (blue curve). Right: SWAXS pattern of CBP-2Si$_3$ in the mesophase at 20 °C, after subtraction of the 43% liquid phase amount present in the pristine state; Figure S9: Absorption and emission (under excitation at 310 nm) spectra of the CBP derivatives in solution (10–5 M in dichloromethane); Figure S10: Potential energy landscape of the CBP-2Si$_3$ molecule calculated at the DFT level by varying the torsion angle between the two N-phenylcarbazole units; Table S1: Structural parameters for the CBP layers in the lamellar phases; Table S2: Siloxane layer configurations in the nanosegregated phases. Refs. [17,27,38] are cited in the Supplementary Materials.

Author Contributions: Conceptualization, B.H., J.-C.R. and S.M.; methodology, J.S. and S.M.; validation, J.S., B.H. and S.M.; formal analysis, J.S., B.H., L.M. and S.M.; investigation, all authors.; resources, L.M. and S.M.; data curation, S.M.; writing—original draft preparation, B.H. and S.M.; writing—review and editing, all authors.; supervision, S.M.; project administration, S.M.; funding acquisition, L.M. and S.M. All authors have read and agreed to the published version of the manuscript.

Funding: This research was funded by the French National Research Agency (ANR) through the Programme d'Investissement d'Avenir under contract ANR-11-LABX-0058-NIE within the Investissement d'Avenir program ANR-10-IDEX-0002-02.

Institutional Review Board Statement: Not applicable.

Informed Consent Statement: Not applicable.

Data Availability Statement: Data is available in this article and its Supplementary Materials.

Acknowledgments: The authors thank Pohang Accelerator Laboratory (PAL) for giving the opportunity to perform the GIWAXS measurements, MEST, and POSTECH for supporting these experiments, Hyungju Ahn and Wooseop Lee for adjustment and help, and other colleagues from the 9A USAXS beamline for assistance. They are also grateful to the French National Center for Scientific Research (CNRS) through the International Research Project LUX-ERIT. Jean Charles Ribierre acknowledges the support by the "Jean d'Alembert" scholarship funded by the Université Paris Saclay.

Conflicts of Interest: The authors declare no conflict of interest.

Sample Availability: Samples of the compounds CBP-2Si$_3$, CBP-2Si$_n$ and CBP-4Si$_3$ are available from the authors.

References

1. Desiraju, G.R. Crystal Engineering: From Molecule to Crystal. *J. Am. Chem. Soc.* **2013**, *135*, 9952–9967. [CrossRef] [PubMed]
2. Mei, J.; Diao, Y.; Appleton, A.L.; Fang, L.; Bao, Z.J. Integrated Materials Design of Organic Semiconductors for Field-Effect Transistors. *Am. Chem. Soc.* **2013**, *135*, 6724–6746. [CrossRef] [PubMed]
3. Mukherjee, A.; Tothadi, S.; Desiraju, G.R. Halogen Bonds in Crystal Engineering: Like Hydrogen Bonds yet Different. *Acc. Chem. Res.* **2014**, *47*, 2514–2524. [CrossRef] [PubMed]
4. Yao, Z.-F.; Wang, F.-Y.; Pei, J. Control of π–π Stacking via Crystal Engineering in Organic Conjugated Small Molecule Crystals. *Cryst Growth Des.* **2018**, *18*, 7–15. [CrossRef]
5. Lu, F.; Nakanashi, T. Alkyl-π engineering in state control toward versatile optoelectronic soft materials. *Sci. Technol. Adv. Mater.* **2015**, *16*, 014805. [CrossRef]
6. Mei, J.; Bao, Z. Side Chain Engineering in Solution-Processable Conjugated Polymers. *Chem. Mater.* **2014**, *26*, 604–615. [CrossRef]
7. Tschierske, C. Liquid crystal engineering—New complex mesophase structures and their relations to polymer morphologies, nanoscale patterning and crystal engineering. *Chem. Soc. Rev.* **2007**, *36*, 1930–1970. [CrossRef]
8. Meng, B.; Liu, J.; Wang, L. Oligo(ethylene glycol) as side chains of conjugated polymers for optoelectronic applications. *Polym. Chem.* **2020**, *11*, 1261–1270. [CrossRef]
9. Ren, Z.; Yan, S. Polysiloxanes for optoelectronic applications. *Prog. Mater. Sci.* **2016**, *83*, 383–416.
10. Mark, J.E. Some Interesting Things about Polysiloxanes. *Acc. Chem. Res.* **2004**, *37*, 946–953. [CrossRef]
11. Dvornik, R.P. *Silicon-Containing Polymers: The Science and Technology of Their Synthesis and Applications*; Jones, R.J., Ando, W., Chojnowski, J., Eds.; Kluwer Academic Publishers: Dordrecht, The Netherlands, 2000; Chapter 7.
12. Clarson, S.J.; Dodgson, K.; Semlyen, J.A. Studies of cyclic and linear poly(dimethylsiloxanes): 19. Glass transition temperatures and crystallization behavior. *Polymer* **1985**, *26*, 930–934. [CrossRef]
13. *Polymer Data Handbook*, 4th ed.; Brandrup, J.; Immergut, E.H.; Grulke, E.A. (Eds.) John Wiley & Sons: New York, NY, USA, 1999; Chapter VI.
14. Pouget, E.; Tonnar, J.; Lucas, P.; Lacroix-Desmazes, P.; Ganachaud, F.; Boutevin, B. Well-Architectured Poly(dimethylsiloxane)-Containing Copolymers Obtained by Radical Chemistry. *Chem. Rev.* **2010**, *110*, 1233–1277. [CrossRef] [PubMed]
15. Kutsumizu, S.; Kawafuchi, A.; Yamamura, Y.; Udagawa, T.; Otaki, T.; Masuda, M.; Miwa, Y.; Saito, K. Stabilization of Bicontinuous Cubic Phase and Its Two-Sided Nature Produced by Use of Siloxane Tails and Introduction of Molecular Nonsymmetry. *Chem. Eur. J.* **2021**, *27*, 10293–10302. [CrossRef] [PubMed]
16. Guillon, D.; Osipov, M.A.; Méry, S.; Siffert, M.; Nicoud, J.-F.; Bourgogne, C.; Sebastião, P.J. Synclinic-anticlinic phase transition in tilted organosiloxane liquid crystals. *Mat. Chem. A* **2011**, *11*, 2700–2708. [CrossRef]
17. Kamatham, N.; Ibraikulov, O.-A.; Durand, P.; Wang, J.; Boyron, O.; Heinrich, B.; Heiser, T.; Lévêque, P.; Leclerc, N.; Méry, S. On the Impact of Linear Siloxanated Side Chains on the Molecular Self-Assembling and Charge Transport Properties of Conjugated Polymers. *Adv. Funct. Mater.* **2020**, *30*, 2007734. [CrossRef]
18. Kamino, B.A.; Bender, T.P. The use of siloxanes, silsesquioxanes, and silicones in organic semiconducting materials. *Chem. Soc. Rev.* **2013**, *42*, 5119–5130. [CrossRef]
19. Sun, D.; Ren, Z.; Bryce, M.R.; Yan, S. Arylsilanes and siloxanes as optoelectronic materials for organic light-emitting diodes (OLEDs). *J. Mat. Chem. C* **2015**, *3*, 9496–9508. [CrossRef]
20. Funahashi, M.; Yamaoka, M.; Takenami, K.; Sonoda, A. Liquid-crystalline perylene tetracarboxylic bisimide derivatives bearing cyclotetrasiloxane moieties. *J. Mat. Chem. C* **2013**, *1*, 7872–7878. [CrossRef]
21. Roland, T.; Léonard, J.; Hernandez Ramirez, G.; Méry, S.; Yurchenko, O.; Ludwigs, S.; Haacke, S. Sub-100 fs charge transfer in a novel donor-acceptor-donor triad organized in a smectic film. *PCCP* **2012**, *14*, 273–279. [CrossRef]
22. Polkehn, M.; Tamura, H.; Eisenbrandt, P.; Haacke, S.; Méry, S.; Burghardt, I. Molecular Packing Determines Charge Separation in a Liquid Crystalline Bisthiophene–Perylene Diimide Donor–Acceptor Material. *J. Phys. Chem. Lett.* **2016**, *7*, 1327–1334. [CrossRef]
23. Mei, J.; Kim, D.H.; Ayzner, A.L.; Toney, M.F.; Bao, Z. Siloxane-Terminated Solubilizing Side Chains: Bringing Conjugated Polymer Backbones Closer and Boosting Hole Mobilities in Thin-Film Transistors. *J. Am. Chem. Soc.* **2011**, *133*, 20130–20133. [CrossRef]
24. Han, A.-R.; Lee, J.; Lee, H.R.; Lee, J.; Kang, S.-H.; Ahn, H.; Shin, T.J.; Oh, J.H.; Yang, C. Siloxane Side Chains: A Universal Tool for Practical Applications of Organic Field-Effect Transistors. *Macromolecules* **2016**, *49*, 3739–3748. [CrossRef]
25. Zhao, F.; Yuan, Y.; Ding, Y.; Wang, Y.; Wang, X.; Zhang, G.; Gu, X.; Qiu, L. Taming Charge Transport and Mechanical Properties of Conjugated Polymers with Linear Siloxane Side Chains. *Macromolecules* **2021**, *54*, 5440–5450. [CrossRef]
26. Plint, T.G.; Kamino, B.A.; Bender, T.P. Charge Carrier Mobility of Siliconized Liquid Triarylamine Organic Semiconductors by Time-of-Flight Spectroscopy. *J. Phys. Chem. C* **2015**, *119*, 1676–1682. [CrossRef]
27. Ribierre, J.-C.; Bao, L.; Inoue, M.; Schwartz, P.-O.; Kim, J.-H.; Yoshida, K.; Sandanayaka, A.S.D.; Nakanotani, H.; Mager, L.; Méry, S.; et al. Low threshold amplified spontaneous emission and ambipolar charge transport in non-volatile liquid fluorene derivatives. *Chem. Commun.* **2016**, *52*, 3103–3106. [CrossRef] [PubMed]
28. Ghosh, A.; Nakanishi, T. Frontiers of solvent-free functional molecular liquids. *Chem. Commun.* **2017**, *53*, 10344. [CrossRef] [PubMed]
29. Lu, F.; Nakanishi, T. Solvent-Free Luminous Molecular Liquids. *Adv. Opt. Mater.* **2019**, *7*, 1900176. [CrossRef]
30. Ribierre, J.-C.; Mizuno, J.; Hattori, R.; Adachi, C. *Organic Light Emitting Diodes with Liquid Emitters in Functional Organic Liquids*; Nakanishi, T., Ed.; Wiley-VCH: Weinheim, Germany, 2019; Chapter 8.

31. Wong, M.Y.; Zysman-Colman, E. Purely Organic Thermally Activated Delayed Fluorescence Materials for Organic Light-Emitting Diodes. *Adv. Mater.* **2017**, *29*, 1605444. [CrossRef]
32. Uoyama, H.; Goushi, K.; Shizu, K.; Nomura, H.; Adachi, C. Highly efficient organic light-emitting diodes from delayed fluorescence. *Nature* **2012**, *492*, 234. [CrossRef]
33. Fukagawa, H.; Shimizu, T.; Kamada, T.; Yui, S.; Hasegawa, M.; Morii, K.; Yamamoto, T. Highly efficient and stable organic light-emitting diodes with a greatly reduced amount of phosphorescent emitter. *Sci. Rep.* **2015**, *5*, 9855. [CrossRef]
34. Yamada, T.; Suzuki, F.; Goto, A.; Sato, T.; Tanaka, K.; Kaji, H. Revealing bipolar charge-transport property of 4,4′-N,N′-dicarbazolylbiphenyl (CBP) by quantum chemical calculations. *Org. Electron.* **2011**, *12*, 169–178. [CrossRef]
35. Schrögel, P.; Tomkevičiene, A.; Strohriegl, P.; Hoffmann, S.T.; Köhler, A.; Lennartz, C. A series of CBP-derivatives as host materials for blue phosphorescent organic light-emitting diodes. *J. Mat. Chem.* **2011**, *21*, 2266–2273. [CrossRef]
36. Babu, S.S.; Hollamby, M.J.; Aimi, J.; Ozawa, H.; Saeki, A.; Seki, S.; Kobayashi, K.; Hagiwara, K.; Yoshizawa, M.; Möhwald, H.; et al. Nonvolatile liquid anthracenes for facile full-colour luminescence tuning at single blue-light excitation. *Nature Commun.* **2013**, *4*, 1969. [CrossRef] [PubMed]
37. Kasahara, T.; Matsunami, S.; Edura, T.; Oshima, J.; Adachi, C.; Shoji, S.; Mizuno, J. Fabrication and performance evaluation of microfluidic organic light emitting diode. *Sens. Actuators A* **2013**, *195*, 219–223. [CrossRef]
38. Shaya, J.; Correia, G.; Heinrich, B.; Ribierre, J.-C.; Polychronopoulou, K.; Mager, L.; Méry, S. Functionalization of Biphenylcarbazole (CBP) with Siloxane-Hybrid Chains for Solvent-Free Liquid Materials. *Molecules* **2022**, *27*, 89. [CrossRef] [PubMed]
39. Tschierske, C. Micro-segregation, molecular shape and molecular topology—Partners of the design of liquid crystalline materials with complex mesophase morphologies. *J. Mater. Chem.* **2001**, *11*, 2647–2671. [CrossRef]
40. Da Rosa, R.R.; Brose, I.S.; Vilela, G.D.; Merlo, A.A. 3,5-diarylisoxazoles: A New Entry to Soft Crystal Phase. *Mol. Cryst. Liq. Cryst.* **2015**, *612*, 158–168. [CrossRef]
41. Mandle, R.J.; Goodby, J.W. Intercalated soft-crystalline mesophase exhibited by an unsymmetrical twist-bend nematogen. *CrystEngComm* **2016**, *18*, 8794–8802. [CrossRef]
42. Kaafarani, A.O.; El-Ballouli, R.; Trattnig, A.; Fonari Sax, S.; Wex, B.; Risko, C.; Khnayzer, R.S.; Barlow, S.; Patra, D.; Timofeeva, T.V.; et al. Bis(carbazolyl) derivatives of pyrene and tetrahydropyrene: Synthesis, structures, optical properties, electrochemistry, and electroluminescence. *J. Mater. Chem. C* **2013**, *1*, 1638–1650. [CrossRef]
43. Xiao, y.; Su, X.; Sosa-Vargas, L.; Lacaze, E.; Heinrich, B.; Donnio, B.; Kreher, D.; Mathevet, F.; Attias, A.-J. Chemical engineering of donor–acceptor liquid crystalline dyads and triads for the controlled nanostructuration of organic semiconductors. *CrystEngComm* **2016**, *18*, 4787–4798. [CrossRef]
44. Pieper, P.; Russo, V.; Heinrich, B.; Donnio, D.; Deschenaux, R. Liquid-Crystalline Tris[60]fullerodendrimers. *J. Org. Chem.* **2018**, *83*, 3208–3219. [CrossRef] [PubMed]
45. Schmidt, A.; Heinrich, B.; Kirscher, G.; Chaumont, A.; Henry, M.; Kyritsakas, N.; Haketa, Y.; Maeda, H.; Mobian, P. Dipyrrolyldiketonato Titanium(IV) Complexes from Monomeric to Multinuclear Architectures: Synthesis, Stability, and Liquid-Crystal Properties. *Inorg. Chem.* **2020**, *59*, 12802–12816. [CrossRef] [PubMed]
46. Del Giudice, N.; L'Her, M.; Scrafton, E.; Atoini, Y.; Gentile, G.; Heinrich, B.; Berthiot, R.; Aliprandi, A.; Douce, L. Luminescent Ionic Liquid Crystals Based on Naphthalene-Imidazolium Unit. *Eur. J Org. Chem.* **2021**, 2091–2098. [CrossRef]
47. Low, P.J.; Paterson, M.A.J.; Yufit, D.S.; Howard, J.A.K.; Cherryman, J.C.; Tackley, D.R.; Brook, R.; Brown, B. Towards an understanding of structure–property relationships in hole-transport materials: The influence of molecular conformation on oxidation potential in poly(aryl)amines. *J. Mat. Chem.* **2005**, *15*, 2304–2315. [CrossRef]
48. Kawakami, Y.; Aoki, T.; Yamashita, Y.; Hirose, M.; Ishitani, A. Surface modification of poly(methyl methacrylate) film by siloxane graft copolymers. *Macromolecules* **1985**, *18*, 580–582. [CrossRef]
49. Houe, Y.; Tulevski, G.S.; Valint, P.L.; Gardella, J.A. Synthesis and Surface Analysis of Siloxane-Containing Amphiphilic Graft Copolymers, Poly(2-hydroxyethyl methacrylate-g-dimethylsiloxane) and Poly(2,3-dihydroxypropyl methacrylate-g-dimethylsiloxane). *Macromolecules* **2002**, *35*, 5953–5962. [CrossRef]
50. Bagnich, S.A.; Rudnick, A.; Schroegel, P.; Strohriegl, P.; Köhler, A. Triplet energies and excimer formation in meta- and para-linked carbazolebiphenyl matrix materials. *Phil. Trans. R. Soc. A* **2015**, *373*, 20140446. [CrossRef]
51. Ab Rani, M.A.; Borduas, N.; Colquhoun, V.; Hanley, R.; Johnson, H.; Larger, S.; Lickiss, P.D.; Llopis-Mestre, V.; Luu, S.; Mogstad, M.; et al. The potential of methylsiloxanes as solvents for synthetic chemistry applications. *Green Chem.* **2014**, *16*, 1282–1296. [CrossRef]
52. Bagnich, S.A.; Athanasopoulos, S.; Rudnick, A.; Schroegel, P.; Bauer, I.; Greenham, N.C.; Strohriegl, P.; Köhler, A. Excimer Formation by Steric Twisting in Carbazole and Triphenylamine-Based Host Materials. *.J. Phys. Chem. C* **2015**, *119*, 2380–2899. [CrossRef]
53. Gong, S.; He, X.; Chen, Y.; Jiang, Z.; Zhong, C.; Ma, D.; Qin, J.; Yan, C. Simple CBP isomers with high triplet energies for highly efficient blue electrophosphorescence. *J. Mat. Chem.* **2012**, *22*, 2894–2899. [CrossRef]
54. Ribierre, J.-C.; Aoyama, T.; Muto, T.; Imase, Y.; Wada, T. Charge transport properties in liquid carbazole. *Org. Elect.* **2008**, *9*, 396–400. [CrossRef]
55. Ribierre, J.-C.; Ruseckas, A.; Gaudin, O.P.M.; Samuel, I.D.W.; Barcena, H.; Staton, S.V.; Burn, P.L. Effects of thermal annealing on the photophysical properties of bisfluorene-cored dendrimer films. *Org. Elect.* **2009**, *10*, 803–808. [CrossRef]
56. Spano, F.C. The Spectral Signatures of Frenkel Polarons in H- and J-Aggregates. *Acc. Chem. Res.* **2010**, *43*, 429–439. [CrossRef]

57. Adachi, C.; Baldo, M.A.; Forrest, S.R. Electroluminescence mechanisms in organic light emitting devices employing a europium chelate doped in a wide energy gap bipolar conducting host. *J. Appl. Phys.* **2000**, *87*, 8049. [CrossRef]
58. Matsushima, H.; Naka, S.; Okada, H.; Onnagawa, H. Organic electrophosphorescent devices with mixed hole transport material as emission layer. *Curr. Appl. Phys.* **2005**, *5*, 305–308. [CrossRef]
59. Matsusue, N.; Suzuki, Y.; Naito, H. Charge Carrier Transport in Neat Thin Films of Phosphorescent Iridium Complexes. *Jap. J. Appl. Phys.* **2005**, *44*, 3691. [CrossRef]